Hydrol. Earth Syst. Sci. Discuss., https://doi.org/10.5194/hess-2017-316
Manuscript under review for journal Hydrol. Earth Syst. Sci.
Discussion started: 6 July 2017

Hydrology and Earth System Sciences
Open Access
Discussions

MULTI RADAR PERFORMANCE IN THE MIDWESTERN UNITED STATES AT LARGE RANGES

Micheal J. Simpson[1], Neil I. Fox[2]

[1]University of Missouri, School of Natural Resources, Water Resources Program, Department of Soil, Environmental, and Atmospheric Sciences, 203-T ABNR Building, Columbia, Missouri, USA, 65201. Tel: +001 5857604031 Email: mjs5h7@mail.missouri.edu

[2]University of Missouri, School of Natural Resources, Water Resources Program, Department of Soil, Environmental, and Atmospheric Sciences, 332 ABNR Building, Columbia, Missouri, USA, 65201. Tel: +001 5738822144 Email: FoxN@Missouri.edu

Correspondence to: Micheal J. Simpson (mjs5h7@mail.missouri.edu)

Abstract. Since the advent of dual-polarized technology, many studies have been conducted to determine the extent to which the differential reflectivity (ZDR) and specific differential phase shift (KDP) add benefits to estimating rain rates (R) to reflectivity (Z). It has been previously noted that this new technology provides significant improvement to rain rate estimation, but only for ranges within 125 km from the radar. Beyond this range, it is unclear as to whether the National Weather Service conventional R(Z)-Convective algorithm is superior, as little research has investigated radar precipitation estimate performance at large ranges. The current study investigates the performance of three radars, St. Louis (KLSX), Kansas City (KEAX), and Springfield (KSGF), MO, with respect to range, with 15 terrestrial-based tipping bucket gauges served as ground-truth to the radars. Over 1100 hours of precipitation data were analyzed for the current study. It was found that, in general, performance degraded with range beyond, approximately, 150 km from the radar. Probability of detection in addition to bias values decreased, while the false alarm ratios increased as range increased. Bright-band contamination was observed to play a potential role as large increases in the absolute bias and overall error values near 120 km for the cool season, and 150 km in the warm season. The analyses found further our understanding in the strengths and limitations of the Next Generation Radar system overall, and from a seasonal perspective.

Hydrol. Earth Syst. Sci. Discuss., https://doi.org/10.5194/hess-2017-316
Manuscript under review for journal Hydrol. Earth Syst. Sci.
Discussion started: 6 July 2017

1 Introduction

In 2012, the National Weather Service (NWS) began upgrading the Next Generation Radar (NEXRAD) system from single- to dual-polarization. The potential benefits of this upgrade were investigated by the National Severe Storms Laboratory (NSSL) and the Cooperative Institute for Mesoscale Meteorological Studies. These advantages include, but are not limited to, (1) significant improvement in radar rainfall estimation (Ryzhkov et al., 2005; Gourley et al., 2010) through better representation of precipitation shape (Brandes et al., 2002; Gorgucci et al., 2000, 2006), (2) discrimination between solid and liquid precipitation (Zrnic and Ryzhkov, 1996), allowing for better distinction between areas of heavy rain and hail (Park et al., 2009; Giangrande and Ryzhkov, 2008; Cunha et al., 2013), (3) identifying the melting layer position in the radar field (Straka et al., 2000; Park et al., 2009), and (4) calculating drop-size distributions retrieved from measurements of reflectivity (Z), differential reflectivity (ZDR), and specific differential phase shift (KDP) as opposed to using ground-based point located disdrometers (Zhang et al., 2001; Brandes et al., 2004; Anagnostou et al., 2008).

Despite the advantages listed above, there are several sources of uncertainty and challenges that meteorologists and hydrometeorologists currently endure. For example, in order to ensure accuracy in rain-rate (R) estimates, Ryzhkov et al., (2005) stated the (mis)calibration effects should, approximately, be limited between $\pm$1 dBZ in reflectivity, and $\pm$0.2 dB for differential reflectivity. The specific differential phase has been shown the be unaffected by beam blockage and other absolute calibration issues (Zrnic and Ryzhkov, 1999), yet attenuation effects may be amplified at X-band radars where the wavelength of the radar signal is more affected by the size of the hydrometeors (Delrieu et al., 2000; Berne and Uijlenhoet, 2005).

Rain rate retrieval by weather radars is an estimation based upon the dielectric properties of the hydrometeors encountered in the atmosphere. Therefore, there is no direct measurement of rainfall, and this inherently introduces error. Although dual-polarized technology allows for the measurements of not

only Z, but also ZDR and KDP, conflicting studies have been conducted as to whether dual-polarized radar rain rate algorithms have improved estimates over single-polarized radar rain rate algorithms. For example, Gourley et al. (2010) and Cunha et al. (2015) reported that conventional R(Z) algorithms have significantly better bias than algorithms containing ZDR and/or KDP, while others (e.g., Ryzhkov et al., 2013; Simpson et al., 2016) report the opposite. This could be due, at least in part, to the fact that hydrometeor types (e.g., rain versus hail) vary on spatial scales that cannot be easily resolved by even densely gauged networks.

Multiple studies have found that, in general, the performance of radar rain rate estimates decrease as range increases (Smith et al., 1996; Ryzhkov et al., 2003) which is caused, primarily, by degradation of beam quality and broadening of the beam with range. Furthermore, the researchers also discuss how the probability of detection at larger ranges decreases, as the radar beam overshoots shallow, stratiform precipitation, including winter storms. Bright-banding can also play a crucial role in significantly increasing the amount of precipitation estimated by the radar.

Despite these overall disadvantages, studies have shown that radar rainrate algorithms seldom exceed absolute errors on the order of 10 mm h^{-1}. However, many of these studies have looked at a small sample of rain events (on the order of 10-50 hours) (Kitchen and Jackson, 1993; Smith et al., 1996; Ryzhkov et al., 2003; Gourley et al., 2010; Cunha et al., 2013). Additionally, few studies (e.g., Smith et al., 1996; Cunha et al., 2015; Simpson et al., 2016) quantified meteorologically significant statistical measures including the probability of detection and false alarm ratio. In order to get a better understanding of the performance of weather radars on rain rate estimates, more data must be collected over a broad range of precipitation regimes in addition to an overall broad region of interest.

The overarching objective of the current study was to assess the overall performance of three different radars within the state of Missouri at various ranges from the radar, using terrestrial-based tipping bucket gauges as ground-truth data. Radar rain rate estimation algorithms include 55 algorithms

encompassing standard R(Z) relations, in addition to algorithms containing dual-polarization variables including ZDR and KDP. A rain rate echo classification algorithm was also tested for performance in correctly identifying the suitable rain rate algorithm to choose based on the Z, ZDR, and KDP radar fields. The current work expands upon that of Simpson et al. (2016) such that a larger sample of data were analyzed (over 1000 hours of rainfall data from forty-six separate days in 2014) to encompass multiple different precipitation regimes for both summer and winter, with several ground-truth tipping buckets to analyze the performance of three separate radars at varying ranges, and further expanding upon the effects of erroneous precipitation estimates on the overall radar error. Objectives for this study included, (1) statistically analyze the performance of each radar at various ranges (compared against the terrestrial-based gauges), (2) compute (a) the amount of precipitation incorrectly estimated by the radar (quantifying the probability of false detection) and (b) the amount of precipitation incorrectly missed by the radar but measured by the rain gauge, (3) test the overall best radar rain rate algorithm, and (4) perform objectives (1), (2), and (3) while the data is separated into warm and cool seasons.

2 Study area and methods

2.1 Study area

National Weather Service radars from St. Louis (KLSX), Kansas City (KEAX), and Springfield (KSGF), MO are able to scan the majority of the state of Missouri. Because of this, the three aforementioned radars were used to assess overall performance in estimating precipitation for this study. Each radar covered a 200-km radius for which a different number of gauges were within the domain: KLSX, KEAX, and KSGF covered 9, 8, and 5 gauges, respectively (Figure 1).

Missouri is characterized as a continental type of climate, marked by relatively strong seasonality. Furthermore, Missouri is subject to frequent changes in temperature, primarily due to its inland location and its lack of proximity to any large lakes. All of Missouri experiences below-freezing temperatures on a

yearly-basis. For example, the majority of the state experiences, on average, 110 days with temperatures below freezing, while the Bootheel (i.e., southeast region) registers, on average, 70 days of below freezing days. This elaborates upon the typical northwest to southeast warming pattern of temperatures observed in the state. Because of the large variability in temperature, the warm and cool seasons were defined from an agronomic perspective, primarily taking probabilities of freezing into account. Based on the climatological averages of Missouri, from 1983 to 2013, November through April registered average minimum temperatures below freezing, and was considered the cool season, while May through October's minimum average temperature were above freezing and constituted the warm season.

2.2 Rainfall data

Terrestrial-based (ground-truthed) precipitation gauge data were collected from 15 separate weather stations within the Missouri Mesonet, established by the Commercial Agriculture Program of University Extension (Table 1). All precipitation data were recorded in hourly intervals which, ultimately, were aggregated to daily totals from 0 to 0 CST for each day used in the study. Forty-six days for the year of 2014 were analyzed for a total of 1,104 hours for each radar which converts to, approximately, 33,000 radar scans in all. The days were chosen based on availability of data from the National Climate Data Center's (NCDC) Hierarchal Data Storage System (HDSS) for all three radars, in addition to error-free performance notes from each of the gauges used. The dates analyzed were split near evenly between warm (May – October) and cool (November – April), therefore encompassing an overall performance of each of the radars throughout the year with no preferential bias towards rain or snow. Additionally, days were distributed evenly during the summer between convective and stratiform events with a threshold of 38 dBZ (Gamache and Houze, 1982).

Observed precipitation data were collected using Campbell Scientific TE525 tipping buckets located at each of the locations for the study (Table 1). The precipitation gauges have a 15.4-cm orifice which funnels to a fulcrum which registers 0.01 mm of rainfall per tip. The performance of each gauge is

maximized between 0 and 50°C, for which each day of the study's temperature did not exceed. Accuracy in gauge measurements range between -1 to 1%, -3 to 0%, and -5 to 0% for precipitation up to 25.4 mm h^{-1}, 25.4 to 50.8 mm h^{-1}, and 50.8 to 76.2 mm h^{-1}, respectively, which are, primarily, associated with local random errors and errors in tip-counting schemes (Kitchen and Blackall, 1992; Habib et al., 2001). Each tipping bucket is located, approximately, 1 m above the ground in areas clear of buildings and properly maintained vegetation height to mitigate turbulence effects (Habib et al., 1999). These errors were assumed negligible and, therefore, allowed for the gauges to be representative of the true rainfall rate.

2.3 Radar data and radar-rainfall algorithms

Next Generation Radar (NEXRAD) level-II data were retrieved from the NCDC's HDSS. Files were analyzed using the Weather Decision Support System – Integrated Information (WDSS-II) program (Lakshmanan et al., 2007) to assess reflectivity (Z) in addition to dual-polarized radar variables including differential reflectivity (ZDR) and specific differential phase shift (KDP). Three other variables were also generated based on a KDP-based smoothing field (Ryzhkov et al., 2003) for reflectivity, differential reflectivity, and specific differential phase: DSMZ, DZDR, and DKDP, respectively. A rain rate echo classification variable (RREC) was also computed, which chooses whether an R(Z), R(KDP), R(Z,ZDR), or R(ZDR, KDP) algorithm is implemented in estimating rain rates based on the radar fields of Z, ZDR, and KDP (Kessinger et al., 2003).

All seven variables (Z, ZDR, KDP, DSMZ, DZDR, DKDP, and RREC) were converted from their native polar grid to 256 x 256 1-km Cartesian grids, where the lowest radar elevation scans (0.5°) were used to mitigate uncalculated effects from evaporation and wind drift. An average of 5-minute scans were used for each of the variables, which were aggregated to hourly totals to be compared to the hourly tipping-bucket accumulations. The latitude and longitude of each of the 15 gauges were matched with the radar pixel that corresponds to the Cartesian grid such that each quantitative value of the seven radar variables were able to be extracted and used in rain rate calculations. Post-processing rain-rate

148 calculations were conducted using the equations presented by Ryzhkov et al. (2005) (Table 2), which
149 were gathered from multiple studies using disdrometers to derive a relationship between reflectivity,
150 differential reflectivity, and specific differential phase (Bringi and Chandrasekar, 2001; Brandes et al.,
151 2002; Illingworth and Blackman, 2002; Ryzhkov et al., 2003). Standard R(Z) algorithms were also
152 included to test whether the addition of dual-polarized technology to rainfall estimates produced
153 improvement.

154 With the use of both Z, ZDR, KDP, and DSMZ, DZDR, and DKDP fields produced by WDSS-II,
155 the number of algorithms tested was 55. This includes the three standard single-polarized algorithms
156 (stratiform, convective, and tropical) which were calculated using reflectivity R(Z), and then calculated as
157 R(DSMZ), while algorithms 1-6 (R(KDP)) were also calculated as R(DKDP). Algorithms 7-11 (R(Z,
158 ZDR)) were additionally calculated as R(Z, DZDR), R(DSMZ, ZDR), and R(DSMZ, DZDR), while the
159 same four combinations of non- and KDP-smoothed fields were applied to the R(KDP, ZDR) algorithms
160 (12-15).

161 **2.4 Statistical analyses**

162 To test the performance of each algorithm, several statistical analyses were calculated. The
163 average difference (Bias) was calculated as

164 $$Bias = \frac{\sum (R_i - G_i)}{N} \quad (1)$$

165 where R_i is each hourly aggregated radar estimated rainfall amount calculated from one of the 55
166 algorithms, G_i is the hourly aggregated gauge (observed) measurement, and N is the total number of
167 observations which, for this study, was 1,104 hours. A second statistical parameter, the normalized mean
168 bias (NMB), was calculated as

Hydrol. Earth Syst. Sci. Discuss., https://doi.org/10.5194/hess-2017-316
Manuscript under review for journal Hydrol. Earth Syst. Sci.
Discussion started: 6 July 2017

$$NMB = \frac{1}{N}\frac{\sum(R_i - G_i)}{\sum G_i} \quad (2)$$

The normalized mean bias is included in the analyses due to the fact that overestimations (i.e., radar estimates larger than gauge measurements) and underestimations (i.e., radar estimates smaller than gauge measurements) are treated proportionately. This is directly analogous to choosing the mean absolute error (MAE) opposed to the standard deviation as the MAE does not penalize smaller or larger errors, obscuring the overall results (Chai and Draxler, 2014). Bias measurements (Bias and NMB) were calculated to determine whether radar derived rain rates were over- or under-estimated in comparison to the gauges. However, to calculate the overall magnitude of error associated with the performance of the radars, the absolute values of (1) and (2) were performed to yield the mean absolute error (MAE), and normalized standard error (NSE), respectively.

Several other meteorological parameters were calculated, including probability of detection (PoD) which was calculated as

$$PoD = \frac{\sum|R_i \bullet G_i > 0 \,\&\, R_i > 0|}{\sum|G_i|} \quad (3)$$

where the bullet ($\bullet$) indicates "if", to determine how accurate the radars were at correctly detecting precipitation. The probability of detection values range between 0.0 (radar did not detect any precipitation correctly) and 1.0 (radar detected the occurrence of all precipitation 100% correctly). The probability of false detection takes into account the amount of precipitation the radars incorrectly estimated when the gauges recorded zero values, and was calculated as

$$PoFD = \frac{\sum R_i \bullet (G_i = 0 \,\&\, R_i > 0)}{\sum G_i} \quad (4)$$

Conversely, the missed precipitation amount (MPA) is the opposite of the PoFD, such that

$$MPA = \sum R_i \bullet (G_i > 0 \,\&\, R_i = 0) \quad (5)$$

Equations 3, 4, and 5 are scaled by the amount of precipitation measured by the gauges. The total amount of rainfall missed and falsely detected (i.e., numerator) of (3), (4), and (5) were also quantified and reported.

3 Results and discussion

3.1 Individual radar performance: All data

To test the overall performance of each radar, it was necessary to determine the overall best algorithm for each statistical measure. Furthermore, the algorithm that performed the best and worst for each gauge and for each radar was assessed.

3.1.1 KEAX

The overall bias showed that there was a positive bias, peaking near 5.5 mm hr^{-1} at the second gauge for KEAX, approximately 115 km from the radar for both the best and worst performing algorithms (Figure 2). This could correspond to a bright-band signature which caused overestimation in precipitation from the algorithms. The overall worst algorithm, equation 13, an R(ZDR,KDP) relationship, revealed a decreasing trend in bias as the distance from the radar increased. This could be due, at least in part, to the algorithm's utilization of KDP which performs poorly in frozen precipitation (Zrnic and Ryzhkov, 1996), causing the underestimation. Conversely, the algorithm with the lowest bias was an R(Z,ZDR) algorithm (equation 11). There was a maximum in the bias calculations while utilizing equation 11 near 120 km, similar to equation 13, however, there was a more pronounced minimum in the data near 150 km. Furthermore, it appears the data oscillates around a bias value of 0 mm hr^{-1} when using

equation 13. This could be due to ZDR's capability to respond to precipitation shape (Kumjian 2013a, b), which helps to scale the reflectivity portion of the rainfall estimation algorithm to a more accurate value. The normalized mean bias (NMB) reveals the same trend in values for bias but with a decrease in magnitude. It is important to note, however, that the algorithms that tend to perform the worst (e.g., algorithms containing KDP) result in anomalous range responses which would be due, at least in part, to a stronger response to precipitation type.

The absolute bias and normalized standard error (NSE) shows the same maxima in the data at the second gauge (Brunswick) that was present in the bias data. However, a second maxima is located at the fifth gauge at, approximately, 150 km (Linneus), which could be a second bright-band present in the summer data, whereas the first maxima is a bright-band in the winter data. There was also a more pronounced minimum in the NSE results at the fourth gauge, indicating the effects of stratiform as opposed to convective precipitation.

The probability of detection (PoD) results show a large difference in algorithm choice for correctly detecting precipitation. The KDP-smoothed R(Z) convective algorithm, R(DSMZ) convective, performed the best in terms of correctly detecting precipitation, whereas algorithm 1 (KDP1) performed the worst, despite its advantages at large ranges (Zrnic and Ryzhkov, 1996). The increased PoD at the second gauge indicates the definite presence of a bright-band, while the low PoD at, approximately 150 km, indicates overshooting of the beam. This is further aided by the MPA results, as about 225 mm of precipitation was missed by the radar at 150 km, whereas only 100 mm of precipitation was missed by the radar at the second gauge at 120 km. Although equation 11, an R(Z,ZDR) algorithm was superior in terms of the bias, the same algorithm with a KDP-smoothed reflectivity value, R(DSMZ,ZDR) revealed the overall least amount of falsely missed precipitation. However, the summation of the amount of precipitation falsely detected (PoFD) by KEAX showed a larger source of error than the MPA in terms of

234 magnitude. For example, at the second (fifth) gauge, only 100 (225) mm of precipitation was missed by
235 the radar, but over 700 (725) mm of precipitation was incorrectly estimated by the radar.

236

237 **3.1.2 KLSX**

238 Unlike the KEAX data, the gauges used for analyses for the KLSX radar span between 90 – 150
239 km. Furthermore, 5 out of the 8 gauges were located within 10 km of range from one-another, near 140
240 km from the radar, limiting the data available for analyses between 100 and 140 km (Figure 3).

241 The bias and NMB show a relatively modest peak in values near the second gauge of 5 mm hr^{-1},
242 which decreases to approximately 3.6 mm hr^{-1} at the third gauge, 120 km from the radar. The worst
243 performing algorithm, equation 13, was the same R(ZDR,KDP) relation as the worst KEAX bias and
244 NMB data. Additionally, the overall trend of decreasing bias and NMB as distance from the radar
245 increases was noted, presumably due to overshooting effects similar to the KEAX data. Furthermore, the
246 overall negative bias displayed by the best-performing algorithm, equation 11, was similar to the KEAX
247 data as well.

248 The double maxima in the absolute bias graph are present as with the KEAX data, but are not as
249 pronounced. Additionally, the overall minima in the absolute bias for both KEAX and KLSX are at,
250 approximately, 125 km from the radar. However, the relative distance from the radars are the same, where
251 the two maxima for KEAX were at 115 and 150 km, while the maxima were at, approximately, 100 and
252 140 km. The overall best and worst performing algorithms for the absolute bias and NSE were equations
253 11 and 13, the R(Z,ZDR) and R(ZDR,KDP) algorithms, respectively.

254 One of the main differences between the KLSX and KEAX data was the decreased probability of
255 detection at 120 km for KLSX, while there was an increased probability of detection for KEAX. In
256 general, the PoD values were worse for KLSX when compared to KEAX. There was also a trend of

257 increasing PoD values as distance from the St. Louis radar increased and, at one point near 140 km, the
258 best algorithm, R(DSMZ) convective and the worst algorithm, KDP1, were not significantly different
259 (10% difference in detection). Additionally, the maxima in the PoD while utilizing KDP1 corresponds to
260 a minima in the R(DSMZ) detection percentage, which is well correlated by the similarly valued MPA
261 results.

262 Another difference between the KEAX and KLSX data was the overall decrease in the PoFD as
263 distance from the radar increased. Because of this, the maxima in the amount of falsely identified
264 precipitation is only 100 km from the radar, which may be effects from bright-banding. Furthermore, this
265 resulted in the overall error in precipitation for algorithm 13 to be in excess of 1,500 mm, while algorithm
266 11 did not exceed 500 mm for the 1,104-hour dataset for KLSX.

267

268 **3.1.3 KSGF**

269 Although the KLSX and KEAX data strongly suggests bright-banding signatures near
270 approximately 100 km and 150 km from the radar, the KSGF results reveal an overall increase of error
271 with range (Figure 4). One of the main reasons for this could be due to the fact that the gauge furthest
272 from any radar analyzed is Cook Station, 185 km from KSGF, which is the range where Ryzhkov et al.
273 (2003, 2005) reported significant fallout in radar performance in rainfall estimation.

274 Overall, the absolute bias values for KLSX, KEAX, and KSGF were within $\pm$ 2 from 6 mm hr^{-1}
275 for the worst performing algorithm, equation 13. However, the radar at Springfield, MO revealed the
276 maximum absolute bias was the furthest gauge at, approximately, 185 km (Cook Station). Although a
277 slight bright-band effect is evident at the second gauge, 100 km from KSGF, the first bright-band is not as
278 evident when compared to the KEAX and KLSX data. However, the overshooting of the beam is more
279 pronounced between 140- and 160-km from KSGF. For example, there is a sharp decrease in the
280 probability of detection within this range, correlating with a decrease in the bias and NMB. Furthermore,

there is an increase in the magnitude of the FAR, indicating a large portion of precipitation was no captured by the radar beam.

3.2 Individual radar performance: Seasonal data

In order to achieve a better understanding of the minimum and maximum values portrayed by the data, all of the radar scans and gauge data were divided into summer (May – October) and winter (November – April) months based on the average climatology of Missouri. This resulted in 652 hours of data for summer, and 452 hours for winter (59 and 41% of the entire data, respectively). Because of this, the overall error is more weighted towards the summer data than the winter data.

The Kansas City bias and absolute bias summer data (Figure 5) shows a similarity to the overall data (Figure 2) in terms of both trend and magnitude. Also, the best performing algorithm for the probability of detection (equation 11) was the same for the summer and overall data. However, the R(Z) Tropical algorithm showed the least reliability in correctly detecting precipitation for the summer, resulting in a more pronounced decrease in the PoD percentage overall. For the NMB and NSE data, the same algorithms that performed best and worse for the overall data (equations 11 and 13) were the best and worst for summer, respectively, and showed similar magnitudes and trends. Conversely, the winter data (Figure 6) showed a pronounced overestimation in the NMB and NSE at the third gauge (125 km) from the radar, with values exceeding 30 mm hr^{-1} compared to values below 6 mm hr^{-1} for the combined seasonal data. This could be due, at least in part, to the large amount of precipitation overestimated by the radar relative to the total amount of precipitation. For example, winter precipitation amounts are significantly lower than convective summertime amounts and, thus, result in a small denominator in (2), leading to an increase in bias. These trends in the KEAX higher NMB and NSE values can be observed for the KLSX and KSGF data as well (Figures 7 and 8, respectively). However, the magnitudes of NMB and NSE were smaller for KSGF in comparison to KLSX and KEAX.

Summing the amount of precipitation not recorded by the radar but recorded by the gauge (MPA) showed similar results when compared between summer and the overall data, but also revealed little contribution of the overall amount from the winter data. Additionally, the best and worst algorithms for the MPA (equations 10 and 14, respectively) were not significantly different ($p = 0.05$). Furthermore, the relatively small contribution from the winter data to the amount of precipitation not estimated by the gauge but estimated by the radar (30 and 40 mm for KLSX and KSGF, respectively) was similar to the KEAX data. The contributions of winter MPA to the overall MPA for all three radars were, approximately, 20%. Conversely, the total amount of precipitation recorded by the radar but not recorded by the gauge (PoFD) showed a relatively large portion from the winter data as opposed to the summer data, with the noticeable exception of the bright-banding effects at the second and fifth gauges (120 and 150 km, respectively) for KEAX. Overall, the winter contribution to the overall PoFD was about 50%.

Overall, the summation of all errors from the radar, including MPA, PoFD, and the absolute bias reveals that, approximately, 20-30% of the error was due to the winter data while comprising 41% of the entire dataset for all three radars. Conversely, the bulk of the error (80%) was due to the 59% total summer results, primarily due to the overall larger magnitudes in rainfall from convective storms. This is further exemplified via Figure 9, showing a scatterplot of all gauge versus radar comparisons. With the exception of a few data points for KEAX, seldom does the winter radar estimated precipitation exceed 10 mm hr^{-1}, while no gauge recorded precipitation exceeded 10 mm hr^{-1}. It is interesting to note that, with the exception of the KLSX data, the winter correlation coefficient values exceed the summer. This could be due, at least in part, to local random errors (Ciach and Krajewski, 1999a) and the excessive (i.e., convective) rainfall that the tipping buckets are unable to accurately measure (Ciach and Krajewski, 1999b; Ciach 2002). Furthermore, because the magnitude of precipitation in the winter is less than the summer, smaller variance and absolute error values are common, causing the correlation coefficient values to be larger than the frequent summertime showers where precipitation values can range from 0 mm hr^{-1} to, in extreme cases, 100 mm hr^{-1}.

330

331 **3.3 Radar performance: Hits only**

332 From the results presented thus far, the majority of the error has resulted from either the PoFD or
333 MPA. Therefore, an analysis into how accurate each algorithm was in comparison to a one-to-one ratio
334 for a correct hit (i.e., gauge and radar recorded precipitation) is presented. This will, in turn, determine
335 whether algorithm 11, an R(Z,ZDR) equation, is still most accurate and whether algorithm 13, an
336 R(ZDR,KDP) equation, is least accurate.

337 From the 55 algorithms possible, the first gauge from each of the three radars (Greenridge,
338 Williamsburg, and Lamar for KEAX, KLSX, and KSGF, respectively), all within 100 km from the radar,
339 showed that either an R(Z) or R(DSMZ) convective algorithm was most accurate with correlation
340 coefficient values around 0.70 (Figures 10-12). Additionally, the second gauge from KEAX (Brunswick)
341 also revealed that an R(Z) convective R^2 value was superior to all other algorithms. For the intermediate
342 gauges from each radar, the rain rate echo classification (RREC) algorithm had the highest correlation
343 coefficient value. For example, for KEAX, St. Joseph (115 km) and Versailles (129 km) had some of the
344 highest R^2 values of 0.62 and 0.88, respectively. For KLSX, the fourth gauge (Bradford, at 135 km from
345 the radar), the RREC correlation coefficient value was 0.55. Beyond, approximately, 140 km from the
346 radar, the KDP3 equation was superior. In fact, the furthest two gauges from each radar showed KDP3 R^2
347 values exceeding 0.40. This could be due, at least in part, to the fact that the specific differential phase
348 does not degrade quality with range, resulting in more accurate results at larger distances (Zrnic and
349 Ryzhkov, 1999; Ryzhkov et al., 2003).

350 For the vast majority of scenarios, DZDRDKDP2 or the R(Z) Tropical algorithms were the worst
351 performing equations. Because the R(Z) Tropical equation was designed for maritime precipitation while
352 this study was conducted in the Midwest, it was not surprising that it was one of the poorest performing
353 algorithms. From the scatterplots of gauge versus radar precipitation (Figures 10-12), when the R(Z)

354 Tropical equation was the worst correlation correlation-valued algorithm, there was, generally,
355 underestimation of precipitation estimated by the radar. Conversely, for the DZDRDKDP algorithm,
356 overestimation of radar estimated precipitation was observed. This could be due to over-smoothing of the
357 ZDR and KDP fields, causing overestimation in rain estimates (Simpson et al., 2016).

358

359

360

361 **4 Conclusions**

362 Dual-polarization technology was implemented to the National Weather Service Next Generation
363 Radar network in the Spring of 2012 to, primarily, improve precipitation estimation and hydrometeor
364 classification. Since this time, a number of studies have been conducted to determine whether this
365 upgrade has improved radar performance in a meteorological, and hydrometeorological sense. Many
366 studies have observed an improvement of radar-based precipitation estimation compared to terrestrial-
367 based precipitation monitors (e.g., Ryzhkov et al., 2003, 2005; Simpson et al., 2016), while other studies
368 show ambiguity between whether there is improvement (e.g., Gourley et al., 2010; Cunha et al., 2015).
369 This study observed over 1,100 hours of precipitation data with three separate radars in Missouri using 55
370 algorithms including the three conventional R(Z) radar rain-rate estimation algorithms (stratiform,
371 convective, and tropical) along with a myriad of R(KDP), R(Z,ZDR), and R(ZDR,KDP) algorithms
372 which can be found in Ryzhkov et al. (2005). Additionally, a KDP-smoothing field of reflectivity,
373 differential reflectivity, and the specific differential phase shift (DSMZ, DZDR, and DKDP, respectively)
374 were measured and used for analyses. Unlike previous studies, the current work emphasizes the amount
375 of precipitation correctly and incorrectly estimated by the radar in comparison to the terrestrial based
376 precipitation gauges through measurements of the probability of detection, probability of false detection,
377 and missed precipitation amount.

For all three radars, Kansas City, St. Louis, and Springfield, MO (KEAX, KLSX, and KSGF, respectively), the vast majority of precipitation error (over 60%) was contributed by the amount of precipitation falsely detection by the radar (up to 725 mm), while 20% was due to the radar missing the precipitation (up to 225 mm) for KEAX. Similar magnitudes of error were reported for KLSX and KSGF, with an overall error in precipitation for each radar ranging between 250 mm for the best performing of the 55 algorithms, equation 11 (an R(Z,ZDR) algorithm), and up to 2000 mm for the worst performing algorithms, R(ZDR,KDP) equation 13.

Radar performance in different seasons has been shown to be significantly different, therefore, the data was divided into summer (May – October) and winter (November – April) months resulting in 652 hours for summer, and 452 hours for winter (59 and 41% of the entire data, respectively). Despite the winter data contributing less than the summertime data, it accounted for 20% of the overall MPA, and 40% to the overall PoFD. The best and worst performing algorithms were the same for the summer and winter data as the overall data, R(Z,ZDR) equation 11 and R(ZDR,KDP) equation 13, respectively.

The overall data was further subdivided into correct radar hits (radar correctly estimated precipitation to be present while the terrestrial based gauge recorded precipitation) for the 1,100-hour dataset. It was found that within 100 km from each of the three radars, the R(Z) or R(DSMZ) convective algorithm revealed the best correlation coefficient values of, approximately, 0.70. Further from the radar, beyond 135 km, RKDP3 generally performed the best due to the algorithms non-degrading capabilities and immunity to beam blockage, whereas at intermediate distances (between 100 and 135 km from the radars), the rain rate echo classification algorithm performed the best. Overall, the worst performing equations were either the R(Z) tropical, or DZDRDKDP2.

These results help our understanding in the possibilities for hydrometeorological studies. Although a mixture of R(Z) convective and R(KDP) algorithms performed the best when precipitation was correctly estimated by the radar, nearly 50% of the 1,100 hours analyzed for the study consisted of

either falsely estimated precipitation by the radar, or missed by the radar. Furthermore, these errors accumulate between 500 to 2,000 mm of precipitation depending on the algorithms chosen. Because of this, a significant source of error and uncertainty must be overcome before radar data can be fully implemented into hydrologic models, especially on a continuous, operational basis.

Author Contribution. N. Fox designed the experiment and provided feedback while M. Simpson carried out the calculations and wrote the manuscript.

Acknowledgements. This material is based upon work supported by the National Science Foundation under Award Number IIA-1355406. Any opinions, findings, and conclusions or recommendations expressed in this material are those of the authors and do not necessarily reflect the views of the National Science Foundation.

References

Anagnostou, M.N., Anagnostou, E.N., Vulpiani, G., Montopoli, M., Marzano, F.S., Vivekanandan, J.: Evaluation of X-band polarimetric-radar estimates of drop-size distributions from coincident S-band polarimetric estimated and measured raindrop spectra. IEEE Transactions on Geoscience and Remote Sensing, 46, 3067-3075, 2008.

Berne, A. and Uijlenhoet, R.: A stochastic model of range profiles of raindrop size distributions: application to radar attenuation correction, Geophysical Research Letters, 32, doi:10.1029/2004GL021899, 2005.

Berne, A. and Krajewski, W.F.: Radar for hydrology: Unfulfilled promise or unrecognized potential? Advances in Water Resources, 51, 357-366, 2013.

424 Bringi, V.N. and Chandrasekar, V.: Polarimetric Doppler weather radar, principles and applications.
425 Cambridge University Press: Cambridge, UK, 636, 2001.

426 Brandes, E.A., Zhang, G., Vivekanandan, J.: Experiments in rainfall estimation with a polarimetric radar in
427 a subtropical environment, Journal of Applied Meteorology, 41, 674–685, 2002.

428 Brandes, E.A., Zhang, G., Vivekanandan, J.: Drop size distribution retrieval with polarimetric radar: model
429 and application, Journal of Applied Meteorology, 43, 461-475, 2004.

430 Chai, T., Draxler, R.R.: Root mean square error (RMSE) or mean absolute error (MAE)? – Arguments
431 against avoiding RMSE in the literature, Geoscientific Model Development, 7, 1247-1250, 2014.

432 Ciach, G.J., Krajewski, W.F.: On the estimation of radar rainfall error variance. Advances in Water
433 Resources, 22, 585-595, 1999a.

434 Ciach, G.J. and Krajewski, W.F.: Radar-raingage comparisons under observational uncertainties. Journal
435 of Applied Meteorology, 38, 1519-1525, 1999b.

436 Ciach, G.J.: Local random errors in tipping-bucket rain gauge measurements. Journal of Atmospheric and
437 Oceanic Technology, 20, 752-759, 2002.

438 Cunha, L.K., Smith, J.A., Baeck, M.L., Krajewski, W.F.: An early performance of the NEXRAD dual-
439 polarization radar rainfall estimates for urban flood applications. Weather and Forecasting, 28, 1478-
440 1497, 2013.

441 Cunha, L.K., Smith, J.A., Krajewski, W.F., Baeck, M.L., Seo, B.: NEXRAD NWS polarimetric precipitation
442 product evaluation for IFloods. Journal of Hydrometeorology, 16, 1676-1699, 2015.

443 Delrieu, G., Andrieu, H., Creutin, J.D.: Quantification of path-integrated attenuation for X- and C-band
444 weather radar systems operating in Mediterranean heavy rainfall. Journal of Applied Meteorology, 39,
445 840-850, 2000.

446 Kitchen, M. and Blackall, M.: Representativeness errors in comparisons between radar and gauge
447 measurements of rainfall. Journal of Hydrology, 134, 13–33, 1992.

448 Gamache, J.F. and Houze, R.A.: Mesoscale air motions associated with a tropical squall line. Monthly
449 Weather Review, 110, 118–135, 1982.

450 Giangrande, S.E. and Ryzhkov, A.V.: Estimation of rainfall based on the results of polarimetric echo
451 classification. Journal of Applied Meteorology, 47, 2445-2460, 2008.

452 Gorgucci, E., Scarschilli, G., Chandrasekar, V., Bringi, V.N.: Measurement of mean raindrop shape from
453 polarimetric radar observations. Journal of the Atmospheric Sciences, 57, 3406-3413, 2000.

454 Gorgucci, E., Baldini, L., Chandrasekar, V.: What is the shape of a raindrop? An answer from radar
455 measurements. Journal of the Atmospheric Sciences, 63, 3033-3044, 2006.

456 Gourley, J.J., Giangrande, S.E., Hong, Y., Flamig, Z., Schuur, T., Vrugt, J.: Impacts of polarimetric radar
457 observations on hydrologic simulation. Journal of Hydrometeorology, 11, 781-796, 2010.

458 Habib, E., Krajewski, W.F., Nespor, V., Kruger, A.: Numerical simulation studies of rain gauge data
459 correction due to wind effect. Journal of Geophysical Research, 104, 723–734, 1999.

460 Habib, E., Krajewski, W.F., Kruger, A.: Sampling errors of tipping-bucket rain gauge measurements.
461 Journal of Hydrological Engineering, 6, 159–166, 2001.

462 Illingworth, A. and Blackman, T.M.: The need to represent raindrop size spectra as normalized gamma
463 distributions for the interpretation of polarization radar observations. Journal of Applied Meteorology,
464 41, 286–297, 2002.

465 Kessinger, C., Ellis, S., Van Andel, J.: The radar echo classifier: a fuzzy logic algorithm for theWSR-88D.
466 19th Conf. on Inter. Inf. Proc. Sys. (IIPS) for Meteor., Ocean., and Hydr., Amer. Meteor. Soc., Long Beach,
467 CA, 2003.

468 Kitchen, M. and Jackson, P.M.: Weather radar performance at long range – simulated and observed.
469 Journal of Applied Meteorology, 32, 975-985, 1993.

470 Kumjian, M.R.: Principles and applications of dual-poarization weather radar. Part 1: Description of the
471 polarimetric radar variables. Journal of Operational Meteorology, 1, 226-242, 2013a.

472 Kumjian, M.R.: Principles and applications of dual-poarization weather radar. Part 2: Warm and cold
473 season applications. Journal of Operational Meteorology, 1, 243-264, 2013b.

474 Kumjian, M.R.: Principles and applications of dual-poarization weather radar. Part 3: Artifacts. Journal of
475 Operational Meteorology, 1, 265-274, 2013c.

476 Lakshmanan, V., Smith, T., Stumpf, G., Hondl, K.: The warning decision support system—integrated
477 information. Weather and Forecasting, 22, 596–612, 2007.

478 Park, H.S., Ryzhkov, A.V., Zrnic, D.S.: The hydrometeor classification algorithm for the polarimetric WSR-
479 88DL Description and application to an MCS. Weather and Forecasting, 24, 730-748, 2009.

480 Ryzhkov, A.V., Giangrande, S., Schurr, T.: Rainfall measurements with the polarimetric WSR-88D radar.
481 National Severe Storms Laboratory Rep. Norman: OK, 98, 2003.

Ryzhkov, A.V., Giangrande, S., Schurr, T.: Rainfall estimation with a polarimetric prototype of WSR-88D. Journal of Applied Meteorology, 44, 502–515, 2005.

Simpson, M.J., Hubbart, J.A., Fox, N.I.: Ground truthed performance of single and dual-polarized radar rain rates at large ranges. Hydrological Processes, 30, 3692-3703, 2016.

Smith, J.A., Seo, D.J., Baeck, M.L., Hudlow, M.D.: An intercomparison study of NEXRAD precipitation estimates. Water Resources Research, 32, 2035-2045, 1996.

Straka, J.M., Zrnic, D.S., Ryzhkov, A.V.: Bulk hydrometeor classification and quantification using polarimetric radar data: Synthesis of relations. Journal of Applied Meteorology, 39, 1341-1372, 2000.

Zhang, G., Vivekanandan, J., Brandes, E.A.: A method for estimating rain rate and drop size distribution from polarimetric radar measurements. IEEE Transactions on Geoscience and Remote Sensing, 39, 830-841, 2001.

Zrnic, D.S., Ryzhkov, A.V.: Advantages of rain measurements using specific differential phase. Journal of Atmosphere and Oceanic Technology, 13, 454-464, 1996.

Zrnic, D.S., Ryzhkov, A.V.: Polarimetry for weather surveillance radars. Bulletin of American Meteorological Society, 80, 389-406, 1999.

506
507
508
509
510
511
512
513
514
515
516
517

518 Table 1. Terrestrial-based precipitation gauge locations used for the study in addition to the National
519 Weather Service Radars Springfield, MO (KSGF), Kansas City, MO (KEAX), and St. Louis, MO
520 (KLSX) used in conjunction with each gauge.

Gauge Location	Latitude (°N)	Longitude (°W)	Radar(s) Used
Bradford	38.897236	-92.218070	KLSX, KEAX
Brunswick	39.412667	-93.196500	KEAX
Capen Park	38.929237	-92.321297	KLSX, KEAX
Cook Station	37.797945	-91.429645	KLSX, KSGF
Green Ridge	38.621147	-93.416652	KEAX, KSGF
Jefferson Farm	38.906992	-92.269976	KLSX, KEAX
Lamar	37.493366	-94.318185	KSGF

Linneus	39.856919	-93.149726	KEAX
Monroe City	39.635314	-91.725370	KLSX
Mountain Grove	37.153865	-92.268831	KSGF
Sanborn Field	38.942301	-92.320395	KLSX, KEAX
St. Joseph	39.757821	-94.794567	KEAX
Vandalia	39.302300	-91.513000	KLSX
Versailles	38.434700	-92.853733	KEAX, KSGF
Williamsburg	38.907350	-91.734210	KLSX

521

522

523

524

525

526 Table 2. List of single- and dual-polarimetric algorithms used for radar rainfall estimates.

$R(Z) = aZ^b$			
Precipitation type	a	b	c
Stratiform	200	1.6	-
Convective	300	1.4	-
Tropical	250	1.2	-
$R(KDP) = a \mid KDP \mid^b sign(KDP)$			
Algorithm number			
1	50.7	0.85	-

2	54.3	0.81	-
3	51.6	0.71	-
4	44.0	0.82	-
5	50.3	0.81	-
6	47.3	0.79	-
$R(Z, ZDR) = aZ^b ZDR^c$			
Algorithm number			
7	6.70×10^{-3}	0.927	-3.43
8	7.46×10^{-3}	0.945	-4.76
9	1.42×10^{-2}	0.770	-1.67
10	1.59×10^{-2}	0.737	-1.03
11	1.44×10^{-2}	0.761	-1.51
$R(ZDR, KDP) = a \mid KDP \mid^b ZDR^c sign(KDP)$			
Algorithm number			
12	90.8	0.930	-1.69
13	136	0.968	-2.86
14	52.9	0.852	-0.53
15	63.3	0.851	-0.72

532

533

534

535

536

537

538

539

540

541

542

543

544 **Figures**

Hydrol. Earth Syst. Sci. Discuss., https://doi.org/10.5194/hess-2017-316
Manuscript under review for journal Hydrol. Earth Syst. Sci.
Discussion started: 6 July 2017

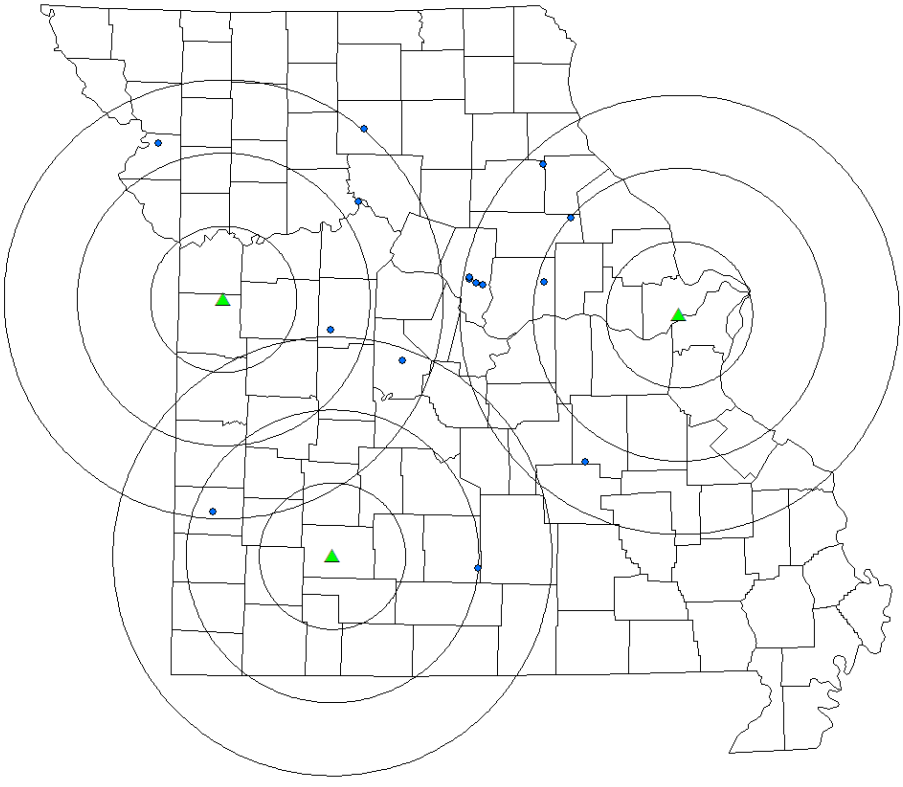

Figure 1. Study location (Missouri) with St. Louis (KLSX), Kansas City (KEAX), and Springfield (KSGF), MO radars (triangles) overlaid with 50-, 100-, and 150-km range rings in addition to the 15 terrestrial-based precipitation gauges utilized as ground-truthed data.

Hydrol. Earth Syst. Sci. Discuss., https://doi.org/10.5194/hess-2017-316
Manuscript under review for journal Hydrol. Earth Syst. Sci.
Discussion started: 6 July 2017

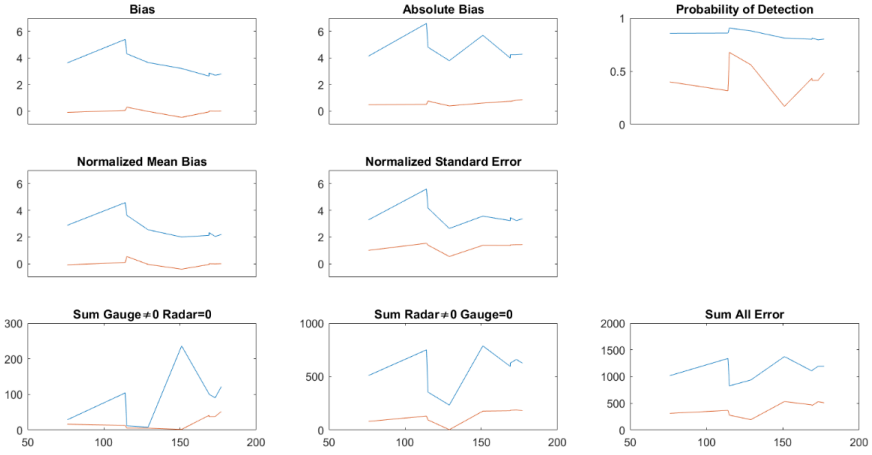

549

550 Figure 2. Overall statistical analyses for the nine gauges used for Kansas City, MO. The blue line
551 represents the weakest performing rain rate estimation algorithm, while the red line represents the overall
552 best performing algorithm for all graphs, with the exception of the probability of detection. All units are
553 in mm hr^{-1} with the exclusion of the probability of detection (unitless).

554

555

556

557

558

559

Hydrol. Earth Syst. Sci. Discuss., https://doi.org/10.5194/hess-2017-316
Manuscript under review for journal Hydrol. Earth Syst. Sci.
Discussion started: 6 July 2017

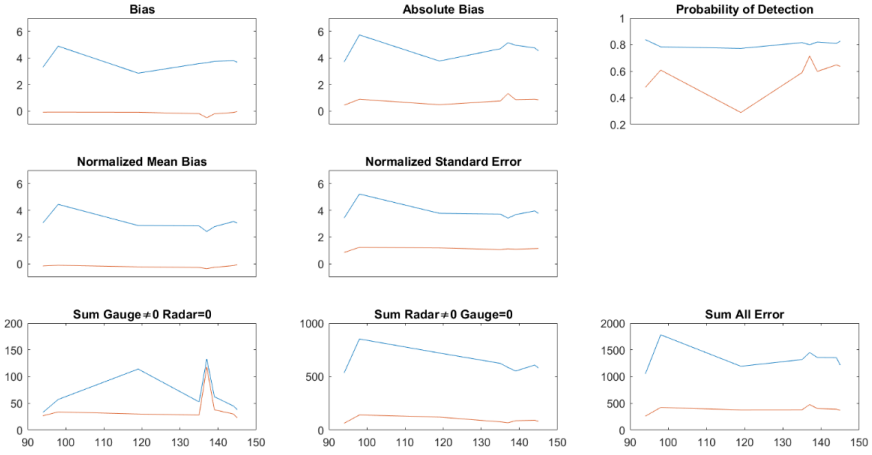

560

561 Figure 3. Overall statistical analyses for the nine gauges used for St. Louis, MO. The blue line represents
562 the weakest performing rain rate estimation algorithm, while the red line represents the overall best
563 performing algorithm for all graphs, with the exception of the probability of detection. All units are in
564 mm hr^{-1} with the exclusion of the probability of detection (unitless).

565

566

567

Hydrol. Earth Syst. Sci. Discuss., https://doi.org/10.5194/hess-2017-316
Manuscript under review for journal Hydrol. Earth Syst. Sci.
Discussion started: 6 July 2017

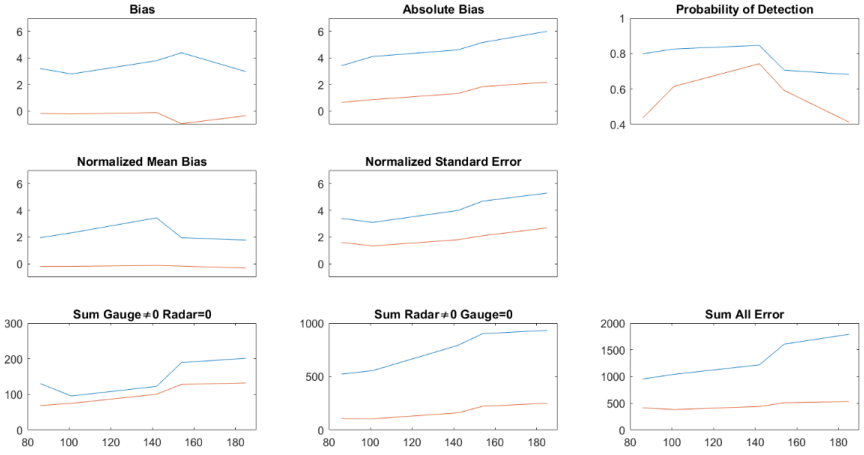

Figure 4. Overall statistical analyses for the nine gauges used for Springfield, MO. The blue line represents the weakest performing rain rate estimation algorithm, while the red line represents the overall best performing algorithm for all graphs, with the exception of the probability of detection. All units are in mm hr^{-1} with the exclusion of the probability of detection (unitless).

Hydrol. Earth Syst. Sci. Discuss., https://doi.org/10.5194/hess-2017-316
Manuscript under review for journal Hydrol. Earth Syst. Sci.
Discussion started: 6 July 2017

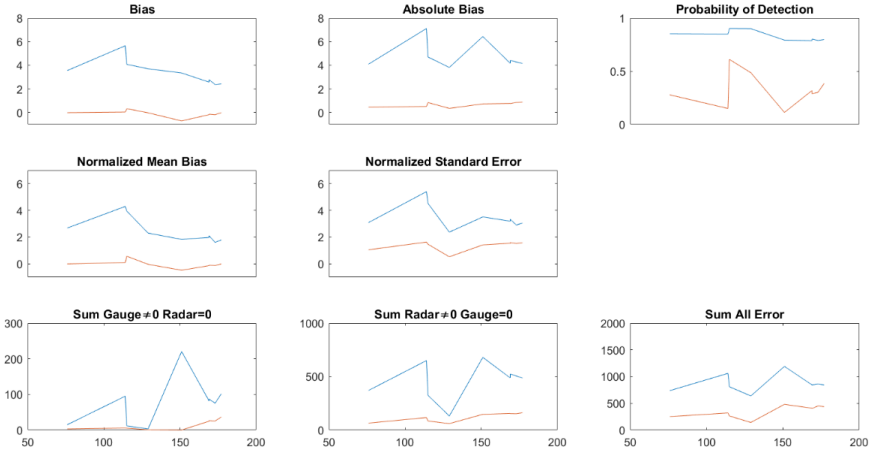

577

578 Figure 5. Statistical analyses for the nine gauges used for Kansas City, MO for warm season data, only.
579 The blue line represents the weakest performing rain rate estimation algorithm, while the red line
580 represents the overall best performing algorithm for all graphs, with the exception of the probability of
581 detection. All units are in mm hr^{-1} with the exclusion of the probability of detection (unitless).

582

583

584

Hydrol. Earth Syst. Sci. Discuss., https://doi.org/10.5194/hess-2017-316
Manuscript under review for journal Hydrol. Earth Syst. Sci.
Discussion started: 6 July 2017

Hydrology and Earth System Sciences
Discussions

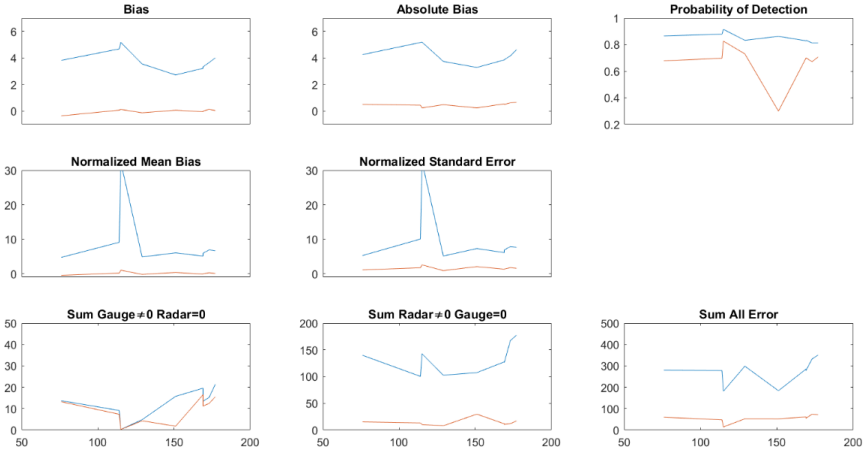

585

586 Figure 6. Statistical analyses for the nine gauges used for Kansas City, MO for cool season analyses, only.
587 The blue line represents the weakest performing rain rate estimation algorithm, while the red line
588 represents the overall best performing algorithm for all graphs, with the exception of the probability of
589 detection. All units are in mm hr^{-1} with the exclusion of the probability of detection (unitless).

590 .

591

592

Hydrol. Earth Syst. Sci. Discuss., https://doi.org/10.5194/hess-2017-316
Manuscript under review for journal Hydrol. Earth Syst. Sci.
Discussion started: 6 July 2017

Hydrology and Earth System Sciences
Discussions

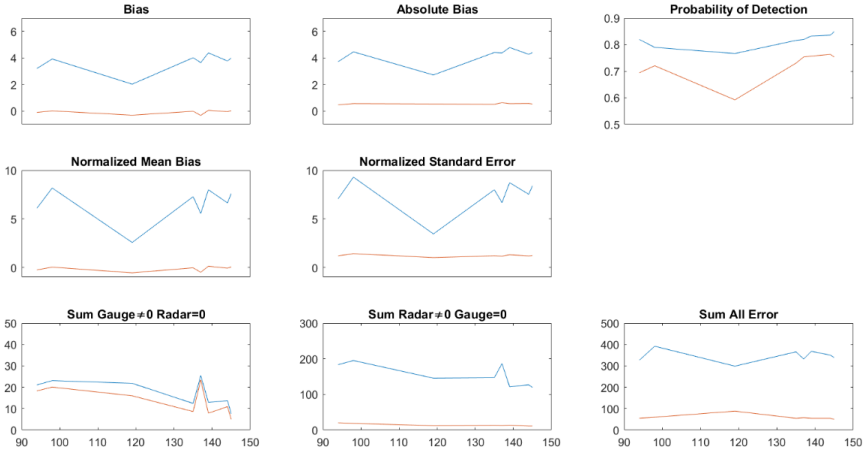

593

594 Figure 7. statistical analyses for the nine gauges used for St. Louis, MO for cool season analyses,
595 only. The blue line represents the weakest performing rain rate estimation algorithm, while the red
596 line represents the overall best performing algorithm for all graphs, with the exception of the
597 probability of detection. All units are in mm hr^{-1} with the exclusion of the probability of detection
598 (unitless).

599

600

Hydrol. Earth Syst. Sci. Discuss., https://doi.org/10.5194/hess-2017-316
Manuscript under review for journal Hydrol. Earth Syst. Sci.
Discussion started: 6 July 2017

Hydrology and Earth System Sciences
Discussions

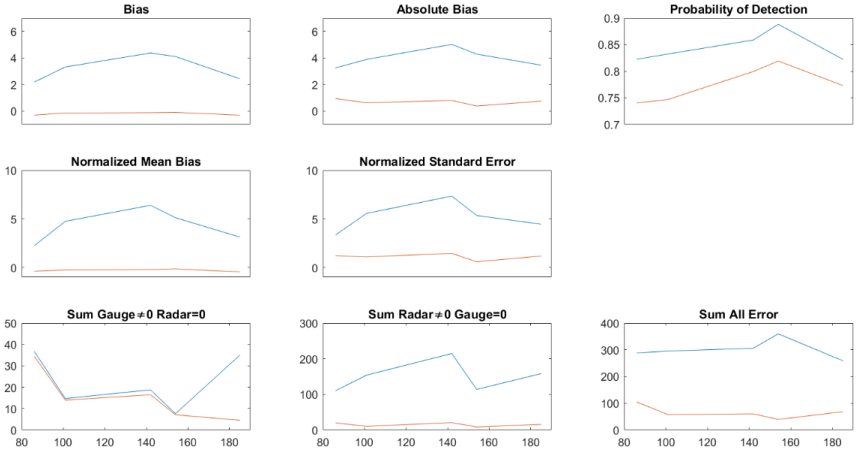

601

602 Figure 8. Statistical analyses for the nine gauges used for Springfield, MO for cool season analyses,
603 only. The blue line represents the weakest performing rain rate estimation algorithm, while the red
604 line represents the overall best performing algorithm for all graphs, with the exception of the
605 probability of detection. All units are in mm hr^{-1} with the exclusion of the probability of detection
606 (unitless).

607

608

609

Hydrol. Earth Syst. Sci. Discuss., https://doi.org/10.5194/hess-2017-316
Manuscript under review for journal Hydrol. Earth Syst. Sci.
Discussion started: 6 July 2017

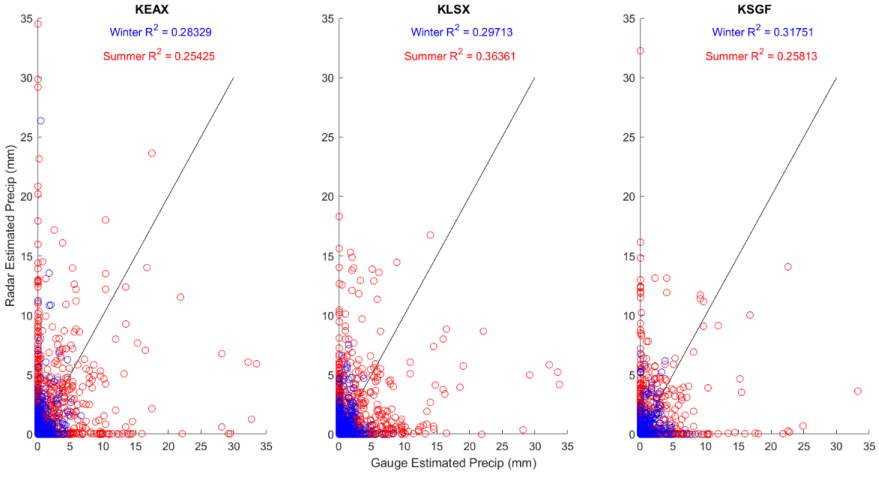

610

611 Figure 9. Scatterplot of gauge estimation precipitation versus radar estimated precipitation with their

612 respective correlation coefficient values for warm and cool seasons.

613

614

615

616

617

618

Hydrol. Earth Syst. Sci. Discuss., https://doi.org/10.5194/hess-2017-316
Manuscript under review for journal Hydrol. Earth Syst. Sci.
Discussion started: 6 July 2017

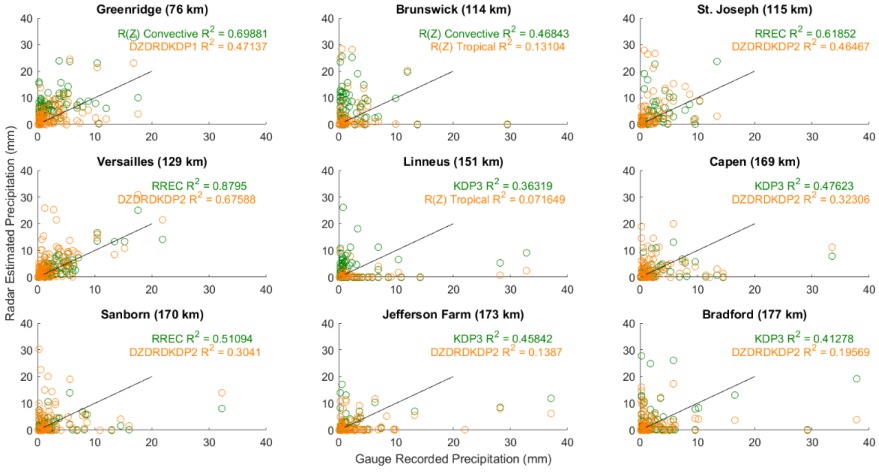

Figure 10. Scatterplots of the best (green) and worst (orange) performing radar rain rate estimation algorithms at each terrestrial based gauge location. Distance from the Kansas City (KEAX) radar is labeled in parenthesis next to the gauge name.

Hydrol. Earth Syst. Sci. Discuss., https://doi.org/10.5194/hess-2017-316
Manuscript under review for journal Hydrol. Earth Syst. Sci.
Discussion started: 6 July 2017

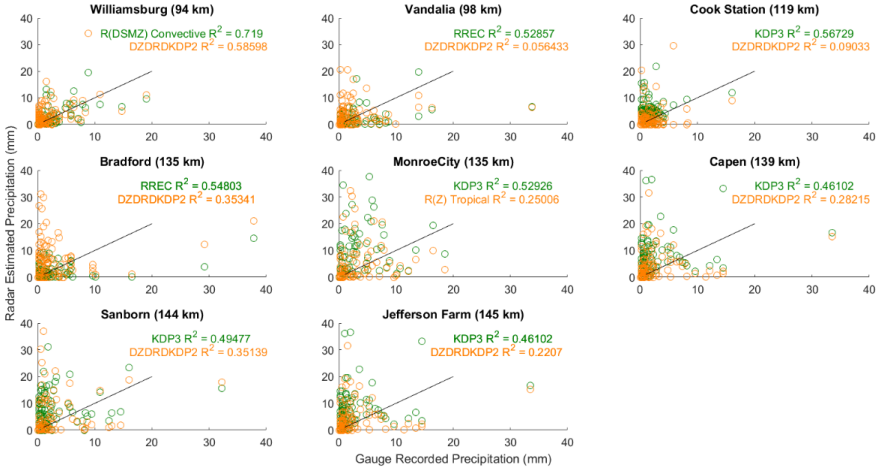

Figure 11. Scatterplots of the best (green) and worst (orange) performing radar rain rate estimation algorithms at each terrestrial based gauge location. Distance from the St. Louis (KLSX) radar is labeled in parenthesis next to the gauge name.

Hydrol. Earth Syst. Sci. Discuss., https://doi.org/10.5194/hess-2017-316
Manuscript under review for journal Hydrol. Earth Syst. Sci.
Discussion started: 6 July 2017

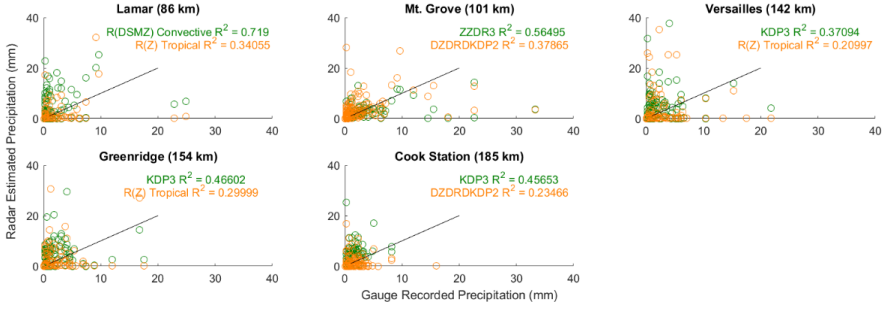

636

637 Figure 12. Scatterplots of the best (green) and worst (orange) performing radar rain rate estimation
638 algorithms at each terrestrial based gauge location. Distance from the Springfield (KSGF) radar is
639 labeled in parenthesis next to the gauge name.